Chaos, Solitons and Fractals 201 (2025) 117285

Contents lists available at ScienceDirect

Chaos, Solitons and Fractals

journal homepage: www.elsevier.com/locate/chaos

Vortex and corner solitons in Stampfli-tiling dodecagonal quasiperiodic lattices

Boquan Ren [a], Yongfeng Qu [a], Milivoj R. Belić [b], Yongdong Li [c], Yiqi Zhang [c,*]

[a] Shaanxi Key Laboratory of Measurement and Control Technology for Oil and Gas Wells, School of Science, Xi'an Shiyou University, Xi'an, 710065, China

[b] College of Science and Engineering, Hamad Bin Khalifa University, 23874 Doha, Qatar

[c] Key Laboratory for Physical Electronics and Devices of the Ministry of Education, School of Electronic and Information Engineering, Xi'an Jiaotong University, Xi'an 710049, China

ARTICLE INFO

Keywords:
Vortex solitons
Quasiperiodic photonic lattice
Stability

ABSTRACT

Quasicrystals are ubiquitous materials that lack translational symmetry but exhibit rotational symmetry. Past studies have demonstrated that quasicrystals offer a promising platform for vortex generation and topological phase transitions. To date, explorations of quasicrystals are diverse, owing to their abundant structures and fascinating properties. Here, we report the existence and stability of thresholdless vortex and corner solitons in Stampfli-tiled dodecagonal quasiperiodic lattices. Theoretical analysis shows that both types of solitons bifurcate from their linear counterparts. Their propagation constants, confined within the bandgap, along with distinct localization characteristics, can be effectively tuned by adjusting the power. According to linear stability analysis and numerical simulations, both vortex and corner solitons exhibit complete stability across their entire existence domains under self-defocusing nonlinearity. By contrast, vortex solitons are stable only at low power levels, while corner solitons display universal instability under self-focusing conditions. These findings provide novel theoretical insights into the behavior of nonlinear waves in quasiperiodic lattices and hold potential for optical information processing and integrated photonic device design.

1. Introduction

Solitons are self-trapped, localized wave packets that arise in nonlinear systems due to a dynamic balance between linear diffraction and nonlinear effects. Characterized by remarkable stability and shape-preserving propagation, solitons have long been a central topic in nonlinear science, with profound implications across physics, mathematics, and engineering [1–8]. In the field of nonlinear optics, localized optical modes, commonly referred to as optical solitons, have attracted sustained attention due to their fundamental significance and wide-ranging applications [9–12], including beam diffraction control [13], logic gate design [14], optical switching devices [15], and information processing [16]. In recent years, extensive research has uncovered a rich variety of soliton families, such as vector [17–19], vortex [20–24], dark [25], spatiotemporal [26,27], fractional solitons [28], each exhibiting distinct spatial structures and topological properties. More recently, the exploration of solitons in complex and structured photonic environments, such as quasiperiodic and aperiodic lattices, has opened new avenues for controlling light propagation and realizing novel localized states with unique symmetry and topological features.

* Corresponding author.
E-mail address: zhangyiqi@xjtu.edu.cn (Y. Zhang).

https://doi.org/10.1016/j.chaos.2025.117285
Received 29 July 2025; Received in revised form 19 September 2025; Accepted 20 September 2025
Available online 28 September 2025

Vortex solitons, as self-trapped wave packets carrying non-zero orbital angular momentum and characterized by phase singularities in their transverse profiles, represent a unique class of localized states in nonlinear systems. The topological charge, defined by the winding number of the phase around the singularity, plays a crucial role in determining their structural and dynamical properties [29]. To date, diverse vortex soliton variants have been identified in various physical settings, including discrete vortex solitons in optically induced photonic lattices [30], higher-order vortex solitons with larger vortex charge [31], necklace and ring-shaped vortex configurations [32], surface vortex states localized at lattice interfaces [33,34], vector vortex solitons with polarization-locked orbital angular momentum [35], and spiraling elliptic solitons with combined azimuthal and radial localization [36].

Such structured solitons have shown significant potential for applications in vortex microlasers [37], optical information encoding [38], all-optical computing, and optical logic gates, among others [39]. Beyond optics, vortex solitons have been reported in ultracold atomic gases, including Bose–Einstein condensates [3,40,41], polaron condensates, plasmas, and nonlinear optical lattices, highlighting broad relevance across multiple branches of physics [10,21,42].

In optical lattice systems, quasiperiodic photonic lattices, which exhibit a spatial order intermediate between perfect periodicity and complete disorder, have emerged as powerful platforms for exploring localized wave dynamics [43–49]. Under Kerr nonlinearity, these systems support localized wave packets with broadened spatial widths [50]. Recent studies further demonstrated that stable solitons can exist in a variety of quasiperiodic structures, including decagonal quasicrystals [51], photonic moiré lattices [52–58], and disclination lattices with defect states [59,60].

Despite growing interest in vortex solitons in quasi-periodic photonic lattices, fundamental questions about their formation mechanisms, stability criteria, and propagation dynamics, remain unresolved. These open issues motivate the present study, which aims to explore the existence, stability, and topological properties of vortex and corner solitons in a Stampfli-tiling-based dodecagonal quasiperiodic photonic lattice.

Here, we systematically investigate optical properties of vortex and corner solitons in Stampfli-tiled dodecagonal quasiperiodic photonic lattices. Our results reveal that corner solitons bifurcate from linear modes and form at lattice corners, while vortex solitons originate from higher-order modes at inner ring lattice sites. Notably, both types of solitons exhibit stability without requiring a power threshold. Under self-defocusing nonlinearity, they demonstrate remarkably wide stability regions. These findings not only reveal the intrinsic physical properties of nonlinear vortex states in quasicrystal structures but also provide a universal theoretical framework for research on localization phenomena in quasiperiodic photonic systems.

The remainder of this work is organized as follows. Section 2 introduces the theoretical model and its band structure. Section 3 deals with the vortex and corner modes of the model. Section 4 presents the stability analysis of the modes found in Section 3, and Section 5 brings conclusions.

2. Theoretical model and band structures

The propagation of a light beam along the z-axis in photonic lattices, particularly those featuring Stampfli-tiling dodecagonal quasicrystal structures, is governed by a dimensionless nonlinear Schrödinger-like equation with focusing/defocusing cubic nonlinearity. This equation accurately describes the evolution of light field amplitude ψ, capturing the interplay between linear waveguiding effects and nonlinear phenomena [61–64]:

$$i\frac{\partial\psi}{\partial z} = -\frac{1}{2}\left(\frac{\partial^2}{\partial x^2} + \frac{\partial^2}{\partial y^2}\right)\psi - \mathcal{R}(x,y)\,\psi - g|\psi|^2\psi. \tag{1}$$

Here, x and y denote the normalized transverse coordinates (with the transverse scale $r_0 = 10\,\mu\text{m}$), while z represents the normalized propagation distance (normalized to diffraction length kr_0, where $k = 2\pi n/\lambda$ is the wavenumber, $\lambda = 800\,\text{nm}$ is the wavelength, and $n = 1.45$ is the refractive index of the material). The parameter $g = +1$ ($g = -1$) corresponds to the focusing (defocusing) nonlinearity. The function $\mathcal{R}(x, y)$ describes the waveguide array, which is z-independent (i.e., the array is straight along the z-axis) and consists of identical waveguides arranged at nodes (x_m, y_n). It is expressed as:

$$\mathcal{R}(x,y) = p\sum_{m,n} e^{-\left[(x-x_m)^2+(y-y_n)^2\right]/\sigma^2}. \tag{2}$$

Here, (x_m, y_n) are lattice site coordinates, $\sigma = 0.5$ is the dimensionless waveguide width and $p = k^2 r_0^2 \delta n/n$ is the lattice depth, proportional to the refractive index modulation depth δn. For a characteristic transverse scale, the chosen parameters $p = 12.0$ and $\delta n \approx 1.3\times10^{-3}$ are typical for femtosecond laser-written waveguide arrays in fused silica [65–69].

The quasicrystalline structure is defined by the polygon edge length $a = 3$ in the lattice. Similar waveguide arrays can be implemented in alternative platforms including photorefractive SBN crystals [70,71] and atomic ensembles [72–74], where the nonlinearity in Eq. (1) may evolve from cubic to saturable type. Numerical simulations confirm that the waveguides with these parameters are single-mode. In Fig. 1(a), we present a photonic quasicrystal structure constructed based on the dodecagonal geometry of the Stampfli tiling, with the waveguide centers positioned at the vertices of this tiling.

This structure exhibits twelve-fold rotational symmetry and is composed of three fundamental units: purple equilateral triangles, yellow squares, and orange rhombuses with a small angle of 30°, all sharing the same side length a. The tiling's large-scale structure is generated via inflation of the original tiles. Unlike the periodic arrangement of conventional crystals, this quasicrystal structure demonstrates long-range order but lacks translational periodicity. The distribution of nodes strictly adheres to the geometric rules of the Stampfli-tiling, fully reflecting its unique structural characteristics. Note that other types of quasiperiodic tilings could have

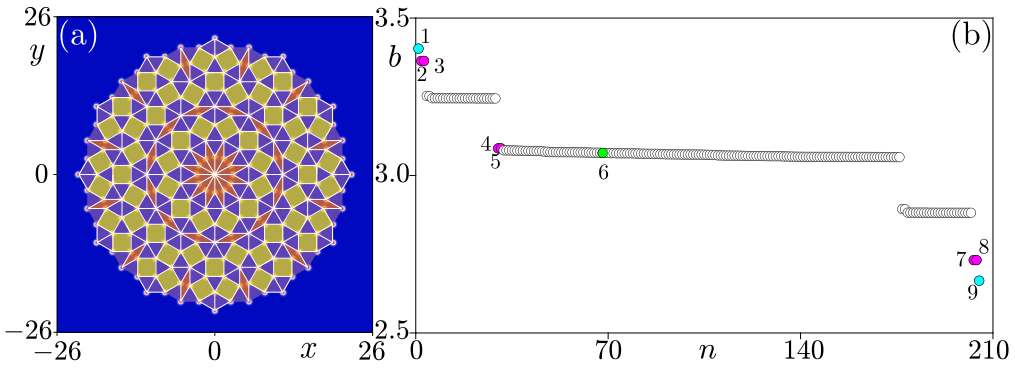

Fig. 1. (a) Stampfli-tiling lattice that is composed of three distinct primitive tiles: square tiles, regular triangle tiles, and rhombus tiles with an acute angle of 30°. These tiles are arranged in a non-periodic but highly symmetric pattern, forming a dodecagonal quasicrystal lattice. (b) Spectrum of the Stampfli-tiling quasicrystal lattice. Cyan, magenta, and green dots correspond to the fundamental, dipole, and corner localized modes, respectively. Black dots are bulk states. (For interpretation of the references to color in this figure legend, the reader is referred to the web version of this article.)

been used in this work, since the focus is on the vortex and corner solitons and not on the structures themselves. However, the lattice chosen offers a wealth of interesting findings on localized states in quasicrystals that warrant publication.

To explore the modes of this type of quasicrystal lattice, we search for the eigenmodes of the structure in the form $\psi = u(x, y)e^{ibz}$, where b is the propagation constant (an eigenvalue) and $u(x, y)$ is the profile of the linear eigenmode. In doing so, we obtain from Eq. (1) the linear eigenvalue problem

$$bu = \frac{1}{2}\left(\frac{\partial^2}{\partial x^2} + \frac{\partial^2}{\partial y^2}\right)u + \mathcal{R}u + gu^3. \tag{3}$$

When we neglect the nonlinear term (by setting $g = 0$ in Eq. (3)), the spectrum of the quasicrystal can be numerically solved using the plane wave expansion method. In this approach, u and $\mathcal{R}$ are expanded into Fourier series with an adequate number of harmonics:

$$u = \sum_{m,n} c_{m,n}\, e^{iK_m x + iK_n y}, \quad \mathcal{R} = \sum_{l,s} v_{l,s}\, e^{iK_l x + iK_s y}, \tag{4}$$

where $c_{m,n}$ and $v_{l,s}$ are the Fourier coefficients, $K_{m,l} = 2(m, l)\pi/D_x$ and $K_{n,s} = 2(n, s)\pi/D_y$ represent reciprocal lattice vectors, $D_{x,y}$ define the computational window dimensions, and (m, n, l, s) are integer indices. Substituting Eq. (4) into the linearized Eq. (3) yields:

$$-\frac{1}{2}(K_m^2 + K_n^2)c_{m,n} + \sum_{l,s} v_{l,s}c_{m-l,n-s} = bc_{m,n}. \tag{5}$$

The system of algebraic equations in Eq. (5) is solved by casting into a matrix form and performing numerical diagonalization, which simultaneously provides the eigenvalue spectrum and the eigenvectors $c_{m,n}$ for constructing different eigenmodes u via Eq. (4). In the calculation process, we set the range of $-30 \le x, y \le 30$ to ensure that the results are not influenced by the boundaries. Fig. 1(b) presents the spectrum of the quasiperiodic photonic lattice with the eigenvalues of $n = 205$ modes with largest propagation constants. In this figure, fundamental, dipole, and corner localized modes are highlighted by colored dots, while bulk states are indicated by blank dots. One finds that the energy spectrum generally exhibits a symmetric structure with respect to its upper and lower boundaries, which is determined by the symmetry of the photonic lattice. Specifically, the linear fundamental and the dipole modes are situated at the upper and lower boundaries of the spectrum, while the eigenmodes of corner states are located within the mid-gap region of bulk states.

The Stampfli-tiling quasicrystal lattice supports several types of modes. Fig. 2 presents the field modulus distributions of some representative linear modes together with their corresponding phase distributions as insets, corresponding respectively to the colored dots in Fig. 1(b). The lattice sites (white circles) are overlaid on these mode fields to clearly visualize the localized distribution of the modes. From the mode profiles, it is evident that the linear modes associated with the cyan and magenta dots are localized within the inner annular region of the quasicrystal photonic lattice, representing the fundamental and dipole modes, respectively. Note that there are two pairs of dipole modes, see modes 2&3 and modes 7&8 in Fig. 2, their phase distributions are different even though they look similar. The phase distributions of modes 1 and 9 in Fig. 2 are also different: one is in-phase and one is out-of-phase.

In contrast, the mode corresponding to the green dot (numbered 6) is localized at the twelve corners of the dodecagonal quasicrystal structure, forming around the outer corners of the finite lattice, i.e., belonging to the class of 0D states. As shown in Fig. 1(b), despite being surrounded by bulk states, the mode demonstrates a distinct corner state localization. In our lattice, there are two fundamental modes (cyan dots), six dipole modes (magenta dots), and one corner state (green dot), and such states are also observed in conventional structures exhibiting rotational symmetry. Additionally, the dipole modes exhibit degeneracy, as exemplified by numbers 2 and 3, numbers 4 and 5, and the pair of states 7 and 8, all of which share identical propagation constants.

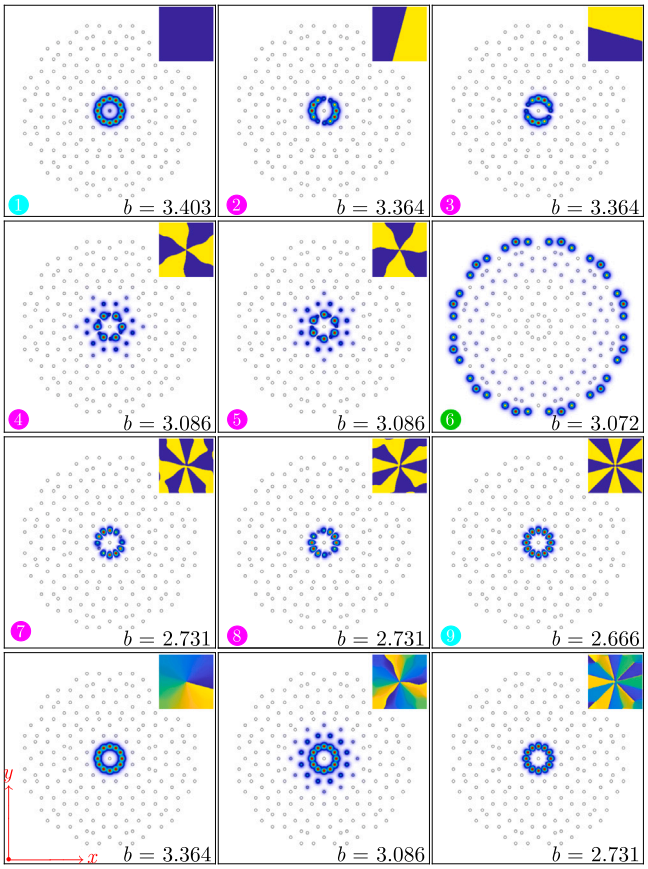

Fig. 2. Field modulus and phase distributions of exemplary states shown within the window $-26 \le x, y \le 26$, with labeled numbers corresponding to those in Fig. 1(b). The inset in each panel shows the phase distribution of the mode (yellow and blue colors represent π 0, respectively), within the window $-5 \le x, y \le 5$. The bottom panels are vortices with the topological charge being 1 (composed of modes labeled 2 and 3), 3 (composed of modes labeled 4 and 5), and 5 (composed of modes labeled 7 and 8), from left to right. (For interpretation of the references to color in this figure legend, the reader is referred to the web version of this article.)

Such states provide a basis for constructing vortex modes. We display these constructed vortex modes in the bottom panels in Fig. 2, with their topological charges being 1, 3, and 5, from left to right. Here, we primarily focus on vortices with a topological charge of 1, as they provide a foundational understanding of the C_{12} symmetric system.

3. Vortex and corner solitons

Linear combinations of degenerate modes can produce vortex states. In the lattice with C_{12} symmetry, only three sets of degenerate states $u_{n=2,3}$, $u_{n=30,31}$, and $u_{n=203,204}$ with identical eigenvalues were found (here n is the index of dipole states depending on the structure size), whose linear combinations $u_{n=2} \pm iu_{n=3}$, $u_{n=30} \pm iu_{n=31}$, and $u_{n=203} \pm iu_{n=204}$ produce vortex modes. Their field modulus occupies all twelve sites within the inner annular region of the lattice. Fig. 2 provides some examples on both the field modulus profiles and corresponding phase distributions of vortex modes in the bottom panels. In this study, we focus on the properties of nonlinear modes generated from linear vortex modes, using the combination $u_{n=2} + iu_{n=3}$, while at the same time exploring the properties of nonlinear corner state solitons in quasicrystal structures under the rotational symmetry.

We consider Kerr nonlinearity of the underlying material and take the steady-state solution of the form

$$\psi(x, y, z) = u(x, y)e^{ibz} = \left[u_r(x, y) + iu_i(x, y)\right] e^{ibz}$$

in Eq. (1) with $g \neq 0$, where $u(x, y)$, $u_r(x, y)$, and $u_i(x, y)$ are the complex, real, and imaginary parts of the solution profile, respectively. The shape of the nonlinear solution $u(x, y)$ corresponding to the propagation constant b is found iteratively, using Newton method. To solve Eq. (3) with the nonlinear term included, we implement a finite difference scheme that transforms the partial differential equation into a system of algebraic equations:

$$f_{m,n}(\mathbf{u}) = \frac{1}{2}\left(\frac{u_{m+1,n} - 2u_{m,n} + u_{m-1,n}}{\Delta x^2} + \right.$$

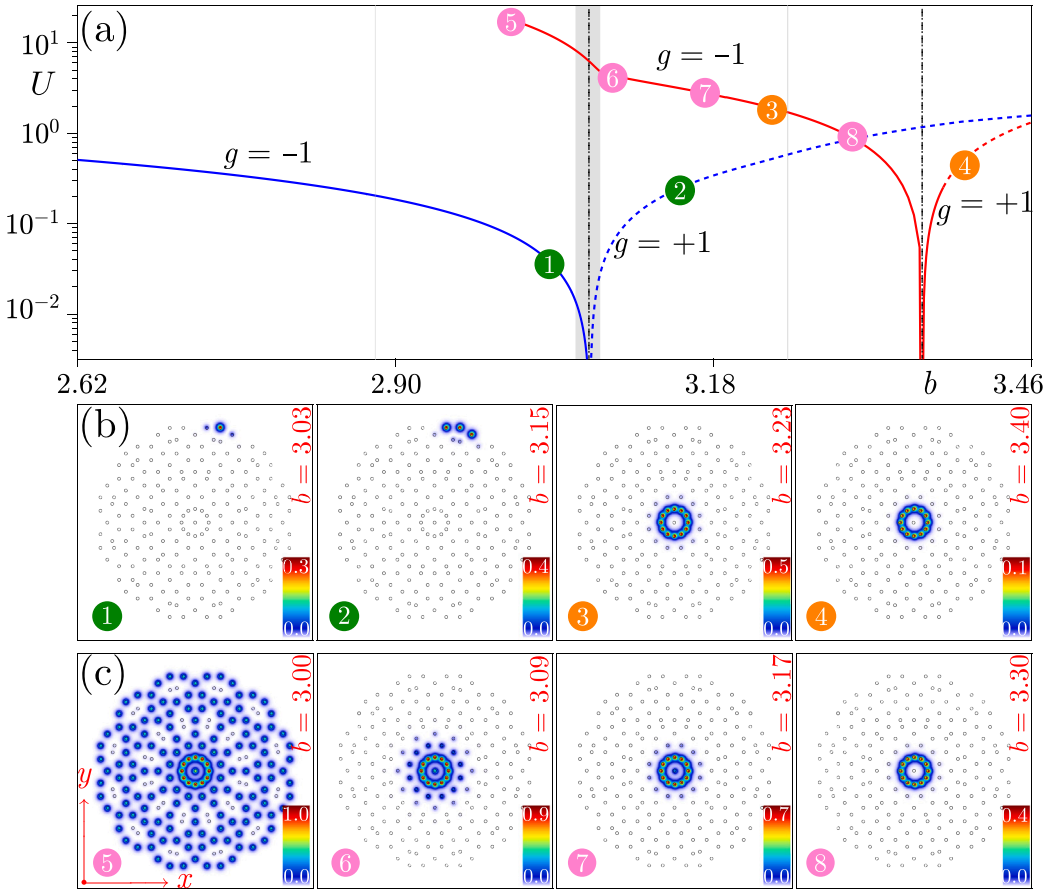

Fig. 3. (a) Families of vortex (red) and corner (blue) solitons in the Stampfli-tiling lattice. Solid/dashed lines indicate stable/unstable branches. Gray area marks bulk bands, with the vertical dashed line marking the location of corner/vortex states. Left ($g = -1$) and right ($g = +1$) sides correspond to self-defocusing and self-focusing nonlinearities. (b) Field modulus distributions of corner solitons that correspond to dots in (a). (c) Field modulus profiles of the vortex soliton with different propagation constant. (For interpretation of the references to color in this figure legend, the reader is referred to the web version of this article.)

$$\left.\frac{u_{m,n+1} - 2u_{m,n} + u_{m,n-1}}{\Delta y^2}\right) + \mathcal{R}_{m,n}u_{m,n} + u_{m,n}^3 - bu_{m,n} = 0, \tag{6}$$

where $\mathbf{u}$ is a vector representing the values of the function $u_{m,n}$ on a numerical grid with spacings $(\Delta x, \Delta y)$. The corresponding Jacobian matrix elements are computed analytically as:

$$J_{(m,n),(p,q)} = \frac{\partial f_{m,n}(\mathbf{u})}{\partial u_{p,q}}. \tag{7}$$

The method entails iteratively solving the associated nonlinear system, to obtain the solution:

$$\mathbf{u}_{\text{new}} = \mathbf{u}_{\text{old}} - \mathbf{J}^{-1}\mathbf{f}, \tag{8}$$

where $\mathbf{f}$ is the vector whose elements are defined by Eq. (6). A stringent convergence criterion $\|\mathbf{u}_{\text{new}} - \mathbf{u}_{\text{old}}\| < 10^{-10}$ ensures numerical precision. Corner solitons can bifurcate from localized linear corner states, supported by the corresponding potential landscape $\mathcal{R}$. Note that similar phenomena can be expected if the nonlinearity of other types is considered.

The families of vortex and corner solitons, obtained by Newton method under focusing ($g = 1$) and defocusing ($g = -1$) nonlinearities, are illustrated in Fig. 3(a). These families are characterized by the dependence of power $U = \iint |\psi|^2 dxdy$ on the propagation constant b, which serves as a free parameter defining the family. The modulus squared $|\psi|^2$ corresponds to the intensity $I = n|\psi|^2/k^2r_0^2n_2$, where n_2 is the nonlinear refractive index of the material. In Fig. 3(a), the red curves represent the families of vortex states, while the blue curves denote the families of corner states. The vertical dash-dotted lines, from left to right, indicate the bands of linear corner and vortex states, respectively, with the gray region representing the bulk states.

The nonlinear corner states in Fig. 3 bifurcate from their corresponding linear counterparts, as indicated by the left vertical dashed line in Fig. 3(a). The vortex solitons bifurcate from the combinations of degenerated modes, and their corresponding propagation constant is indicated by the right vertical dashed line in Fig. 3(a). This indicates that these solitons are thresholdless. Furthermore, the bifurcation point corresponds to the value of b associated with the degenerate linear modes starting to build the corresponding vortex and corner states. Additionally, the power increases significantly as b approaches either the upper or the lower edge of the bandgap. It is observed that the nature of nonlinearity determines the direction of bifurcation: In focusing media, the soliton power U increases with b, whereas in defocusing media, U increases as b decreases. Moreover, the power of nonlinear states exhibits approximately a linear dependence on the propagation constant.

Next, from the curves of the corner soliton family and the self-defocusing vortex soliton family, it is revealed that nonlinear states can exist not only within the bandgap but also in the bulk states. This indicates that the nonlinearity can drive the propagation constant of nonlinear modes into the bulk bands, and the continuation of the same family can be found in higher bandgaps. The shapes of corner and vortex solitons depend on the position of the propagation constant within the energy spectrum. Although corner and vortex solitons are localized at the corners and annular regions of the quasicrystalline photonic lattice, they gradually extend into the bulk of the lattice as the propagation constant approaches the band edges. Specifically, the localization of the state becomes worse and worse as the propagation constant approaches to and finally penetrates into the band. In Fig. 3(c), we explicitly show the field modulus distributions for the defocusing vortex soliton as an example.

Thus, we systematically investigate the properties of solitons by selecting representative nonlinear states from the families of corner and vortex solitons, under both self-focusing and self-defocusing nonlinearities. The field modulus distributions of these states are presented in Fig. 3(b), with their propagation constants corresponding to the characteristic points labeled 1–4 in Fig. 3(a). It is found that, under both focusing and defocusing conditions, the corner solitons bifurcate from their linear counterparts and traverse the gray region associated with the linear bulk states. Within the energy band of the bulk states, the corner states couple with the bulk modes, leading to the delocalization of these modes.

4. Stability analysis

The stability of nonlinear solitons represents an essential part of their study [75,76]. In our work, to investigate the stability of corner and vortex solitons in quasicrystal structures, we introduce a small perturbation (5% of the initial amplitude) into nonlinear states obtained under both self-focusing and self-defocusing conditions. We propagate these perturbed states using Eq. (1) over a distance of $z = 8000$, which exceeds typical sample lengths by several orders of magnitude. For instance, in femtosecond laser written waveguides, a 10 cm sample length corresponds to a dimensionless propagation distance of $z \approx 88$. Consequently, this propagation distance is thus theoretically sufficient to comprehensively assess the stability of nonlinear states.

In the results, as depicted in Fig. 3(a), solid lines represent stable while dashed lines denote unstable soliton families. For corner solitons under self-defocusing nonlinearity ($g = -1$), solitons remain stable throughout their entire domain; whereas under self-focusing nonlinearity ($g = +1$), they remain unstable. Vortex solitons, akin to corner solitons, exhibit complete stability within their existence region under self-defocusing nonlinearity. However, under self-focusing nonlinearity they display only a narrow stable region at low power levels.

These findings are corroborated by the linear stability analysis method, which considers the perturbed solution of Eq. (1) in the form:

$$\psi = [u(x,y) + v(x,y)e^{\delta z} + w^*(x,y)e^{\delta^* z}]e^{ibz} \tag{9}$$

Considering small perturbations $v, w \ll 1$ with complex growth rate δ, we substitute Eq. (9) into Eq. (1) and perform linearization about the stationary solution u, yielding a linear eigenvalue problem:

$$\begin{aligned} i\delta v &= -\frac{1}{2}\left(\frac{\partial}{\partial x^2} + \frac{\partial}{\partial y^2}\right)v - (\mathcal{R} - b)v - 2g|u|^2 v - g|u|^2 w, \\ i\delta w &= +\frac{1}{2}\left(\frac{\partial}{\partial x^2} + \frac{\partial}{\partial y^2}\right)w + (\mathcal{R} - b)w + 2g|u|^2 w + g|u|^2 v. \end{aligned} \tag{10}$$

Using the standard eigenvalue solver for Eq. (10), we determine the dependence of the perturbation growth rate δ on the propagation constant b for each family of nonlinear states. The stability criterion emerges as follows: When $\mathrm{Re}(\delta) \leq 0$ for all perturbation modes, the corresponding nonlinear state u is linearly stable; conversely, if any mode yields $\mathrm{Re}(\delta) > 0$, the state becomes unstable. The results indicate that the stability of the nonlinear states determined using this method is consistent with that obtained from the propagation of states with 5% superimposed noise.

Clearly, to thoroughly investigate unique properties of vortex solitons in quasicrystal photonic lattice structures, we conducted a systematic study. Considering the significant influence of nonlinear conditions on the characteristics of vortex solitons, we selected two distinct nonlinear regimes: Self-defocusing and self-focusing, with propagation constants $b = 3.23$ and $b = 3.40$. In Fig. 3(a), the two orange points labeled 3 and 4 represent vortex solitons under these conditions, respectively. During the study, we propagated the nonlinear states with superimposed noise over a long distance. Throughout the propagation, we recorded the amplitude variations of vortex solitons and monitored the dynamic evolution of their field modulus and phase distributions.

Fig. 4(a) illustrates the evolution of vortex solitons with noise, for the self-defocusing case ($b = 3.23$) shown in Fig. 3(a). In Fig. 4(a), it can be observed that the vortex soliton maintains its profile throughout the long-distance propagation. Fig. 4(c) presents the maximum amplitude $A_{\max}$ of the corresponding vortex soliton along the propagation axis z throughout the propagation process.

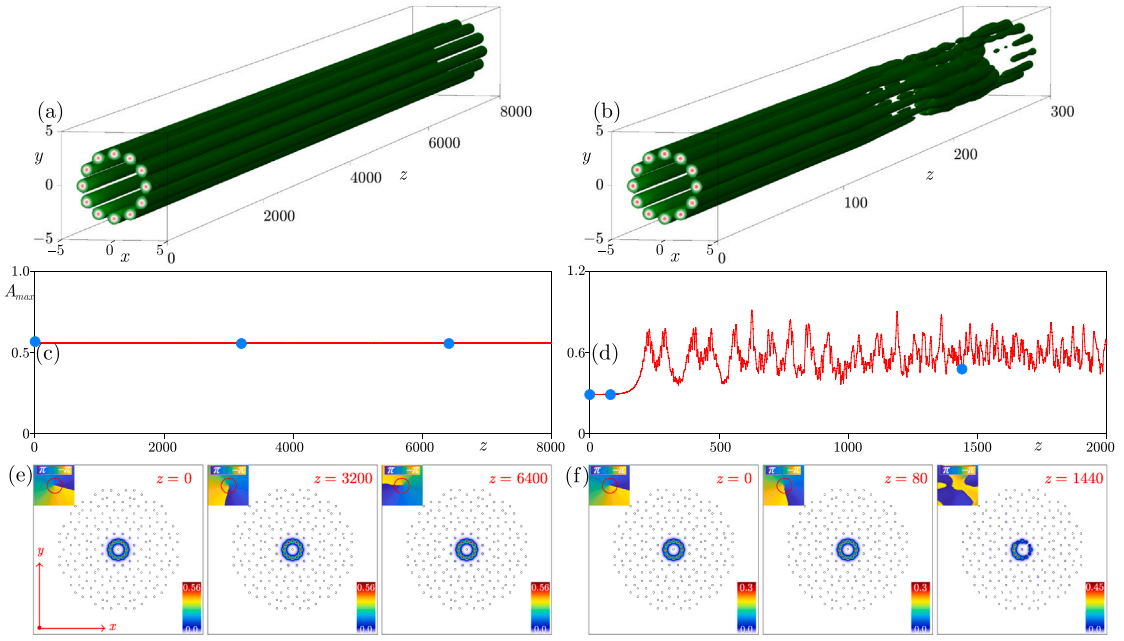

Fig. 4. (a) Propagation dynamics of vortex solitons with $b = 3.23$ at different propagation distances z up to $z = 8000$. (b) Setup is as (a) but for $b = 3.40$ up to $z = 300$. (c,d) Peak amplitude $A_{\max}$ of the vortex solitons in (a,b) during propagation. (e,f) Field modulus distributions of vortex solitons corresponding to the blue dots in (c,d) with insets showing the corresponding phase distributions. In (a,c) $g = +1$, while in (b,d) $g = -1$. (For interpretation of the references to color in this figure legend, the reader is referred to the web version of this article.)

It is evident that the amplitude remains constant during the entire propagation, indicating a strong stability of the vortex soliton under these conditions. Fig. 4(e) presents the field modulus distributions at three specific propagation points [marked in blue in Fig. 4(c)], with the corresponding phase distributions in the inner ring region, shown in the insets in upper left corners. Obviously, the vortex soliton achieves strong localization in the inner annular region of the lattice structure, accompanied by evident phase rotation during propagation, a characteristic feature of vortex beams. Notably, the vortex phase distribution exhibits a phase singularity at the center, highlighted by red circles in phase diagrams, for a clearer observation.

In contrast, the right side displays the propagation of a vortex soliton under the self-focusing nonlinearity ($b = 3.40$) with superimposed noise. Fig. 4(b) shows the amplitude distribution of the vortex soliton for $b = 3.40$. Correspondingly, Fig. 4(d) depicts the max amplitude evolution with propagation distance. Evidently, in the initial propagation stage the vortex soliton (positioned at the twelve lattice points within the inner ring of the quasicrystalline structure) maintains a relatively stable profile, clearly demonstrating stability during this phase. However, as the propagation distance z increases, after $z = 150$ the profile begins to exhibit noticeable irregular variations. This behavior is further confirmed in the field modulus and phase distribution analysis. At $z = 0$ and $z = 80$, the field modulus patterns maintain their original shapes well, with noticeable phase rotation during propagation. However, at $z = 1440$, while the field modulus remains localized in the inner annular region without extending into the bulk (due to the considerable distance between the vortex states and the bulk band region), the field becomes nonuniform at each inner ring position, and the rotating phase structure disappears, clearly indicating the onset of strong (turbulent) instability.

5. Conclusion

In summary, we have demonstrated the existence of vortex solitons and corner soliton families in a dodecagonal quasiperiodic photonic lattice based on Stampfli-tiling. The stability and several unique properties of these solitons were investigated in both self-focusing and self-defocusing nonlinearities. Our research revealed that, in contrast to nonlinear self-sustained states in periodic photonic lattices, the corner and vortex solitons in this aperiodic quasicrystalline structure do not exhibit a power threshold. The absence of threshold power is attributed to the fundamental difference in periodic and aperiodic lattice formation, where the nonlinear self-sustained states in periodic photonic lattices inherently require a minimum power for their establishment.

Furthermore, our research reveals distinct formation mechanisms in both self-focusing and self-defocusing conditions, whereby corner solitons originate from the bifurcation of corner states, while vortex solitons arise from the composition of higher-order modes. Notably, under the self-defocusing nonlinearity, both corner and vortex solitons maintain stability throughout their existence range. In contrast, under self-focusing nonlinear conditions, corner solitons exhibit instability, while vortex solitons maintain stability only within a low-power range. These findings provide valuable insights into the origin and dynamic characteristics of gap solitons in two-dimensional quasiperiodic photonic lattices with defocusing and focusing nonlinearities.

The threshold-free nature of these solitons suggests an applicative potential for low-power optical devices in integrated photonic circuits [77]. The observed vortex solitons could enable high-capacity optical communications through orbital angular momentum multiplexing [78], and the corner states may find applications in topological photonic insulators [79–81]. Moreover, our results establish a theoretical framework for exploring nonlinear localized states in this and similar quasiperiodic structures, in future research.

CRediT authorship contribution statement

Boquan Ren: Writing – original draft, Methodology, Investigation, Formal analysis. **Yongfeng Qu:** Validation, Methodology, Investigation. **Milivoj R. Belić:** Validation, Formal analysis, Conceptualization. **Yongdong Li:** Validation, Investigation. **Yiqi Zhang:** Writing – review & editing, Supervision.

Funding

Boquan Ren is supported by the National Natural Science Foundation of China (12504393). Yiqi Zhang is supported by the Natural Science Basic Research Program of Shaanxi Province (2024JC-JCQN-06, 2025JC-QYCX-006) and the National Natural Science Foundation of China (12474337).

Declaration of competing interest

The authors declare that they have no known competing financial interests or personal relationships that could have appeared to influence the work reported in this paper.

Acknowledgments

Boquan Ren and Yiqi Zhang acknowledge Prof. Hongguang Wang for helpful discussions. All authors acknowledge the anonymous reviewers for their nice suggestions that improve the presentation greatly.

Data availability

Data will be made available on request.

References

[1] Kivshar YS, Agrawal GP. Optical solitons: from fibers to photonic crystals. Academic Press; 2003.
[2] Malomed BA. Multidimensional soliton systems. Adv Phys: X 2024;9(1):2301592.
[3] Mihalache D. Localized structures in optical media and Bose-Einstein condensates: An overview of recent theoretical and experimental results. Rom Rep Phys 2024;76(2):402.
[4] Lederer F, Stegeman GI, Christodoulides DN, Assanto G, Segev M, Silberberg Y. Discrete solitons in optics. Phys Rep 2008;463(1–3):1–126.
[5] Malomed BA. Two-dimensional solitons in nonlocal media: a brief review. Symmetry 2022;14(8):1565.
[6] Malomed BA. A new topic in the studies of topological solitons: Topologically protected higher-order modes in fractal optical systems. Low Temp Phys 2025;51(6):665–70.
[7] Malomed BA. Basic fractional nonlinear-wave models and solitons. Chaos: Interdiscip J Nonlinear Sci 2024;34(2).
[8] Malomed BA. Optical solitons and vortices in fractional media: A mini-review of recent results. Photonics 2021;8(9).
[9] Blanco-Redondo A, de Sterke CM, Xu C, Wabnitz S, Turitsyn SK. The bright prospects of optical solitons after 50 years. Nat Photonics 2023;17(11):937–42.
[10] Kartashov YV, Astrakharchik GE, Malomed BA, Torner L. Frontiers in multidimensional self-trapping of nonlinear fields and matter. Nat Rev Phys 2019;1(3):185–97.
[11] Kartashov YV, Malomed BA, Torner L. Solitons in nonlinear lattices. Rev Modern Phys 2011;83(1):247–305.
[12] Taylor J. Early optical soliton research at Imperial College London. Opt Commun 2023;536:129382.
[13] Zhang Y, Qin Y, Zheng H, Ren H. The evolution of the solitons in periodic photonic Moiré lattices controlled by rotation angle with saturable self-focusing nonlinearity media. Laser Phys 2022;32(4):045401.
[14] Serak SV, Tabiryan NV, Peccianti M, Assanto G. Spatial soliton all-optical logic gates. IEEE Photonics Technol Lett 2006;18(12):1287–9.
[15] Peccianti M, Conti C, Assanto G, De Luca A, Umeton C. All-optical switching and logic gating with spatial solitons in liquid crystals. Appl Phys Lett 2002;81(18):3335.
[16] Rajan MM, Veni SS. Nonautonomous three soliton interactions in an inhomogeneous optical fiber: Application to soliton switching devices. Optik 2023;272:170317.
[17] Shen M, Chen X, Shi J, Wang Q, Krolikowski W. Incoherently coupled vector dipole soliton pairs in nonlocal media. Opt Commun 2009;282(24):4805–9.
[18] Tang Q, Zhang Y, Kartashov YV, Li Y, Konotop VV. Vector valley Hall edge solitons in superhoneycomb lattices. Chaos Solitons Fractals 2022;161:112364.
[19] Tian Y, Wang Y, Belić MR, Zhang Y, Li Y, Ye F. Vector valley Hall edge solitons in distorted type-II Dirac photonic lattices. Opt Express 2023;31(13):20812–24.
[20] Li C, Kartashov YV. Stable vortex solitons sustained by localized gain in a cubic medium. Phys Rev Lett 2024;132(21):213802.
[21] Malomed BA. (INVITED) vortex solitons: Old results and new perspectives. Phys D: Nonlinear Phenom 2019;399:108–37.
[22] Malomed B, Kevrekidis P. Discrete vortex solitons. Phys Rev E 2001;64(2):026601.
[23] Mihalache D, Mazilu D, Lederer F, Leblond H, Malomed B. Stability limits for three-dimensional vortex solitons in the Ginzburg-Landau equation with the cubic-quintic nonlinearity. Phys Rev A 2007;76(4):045803.
[24] Li P, Malomed BA, Mihalache D. Vortex solitons in fractional nonlinear Schrödinger equation with the cubic-quintic nonlinearity. Chaos Solitons Fractals 2020;137:109783.

[25] Ren B, Wang H, Kompanets VO, Kartashov YV, Li Y, Zhang Y. Dark topological valley Hall edge solitons. Nanophotonics 2021;10(13):3559–66.
[26] Mihalache D, Mazilu D, Lederer F, Malomed B, Kartashov YV, Crasovan L-C, Torner L. Stable spatiotemporal solitons in Bessel optical lattices. Phys Rev Lett 2005;95(2):023902.
[27] Malomed BA, Mihalache D, Wise F, Torner L. Spatiotemporal optical solitons. J Opt B: Quantum Semiclass Opt 2005;7(5):R53.
[28] Zeng L, Zhu Y, Malomed BA, Mihalache D, Wang Q, Long H, Cai Y, Lu X, Li J. Quadratic fractional solitons. Chaos Solitons Fractals 2022;154:111586.
[29] Caplan RM, Carretero-González R, Kevrekidis PG, Malomed BA. Existence, stability, and scattering of bright vortices in the cubic–quintic nonlinear Schrödinger equation. Math Comput Simulation 2012;82(7):1150–71.
[30] Neshev DN, Alexander TJ, Ostrovskaya EA, Kivshar YS, Martin H, Makasyuk I, Chen Z. Observation of discrete vortex solitons in optically induced photonic lattices. Phys Rev Lett 2004;92(12):123903.
[31] Zeng L, Wang T, Belić MR, Mihalache D, Zhu X. Higher-order vortex solitons in kerr nonlinear media with a flat-bottom potential. Nonlinear Dynam 2024;112(24):22283–93.
[32] Desyatnikov AS, Kivshar YS. Necklace-ring vector solitons. Phys Rev Lett 2001;87(3):033901.
[33] Kartashov YV, Egorov AA, Vysloukh VA, Torner L. Surface vortex solitons. Opt Express 2006;14(9):4049–57.
[34] Jović D, Jovanović R, Denz C, Belić M. Surface vortex solitons near boundaries of photonic lattices. Phys Scr 2012;2012(T149):014040.
[35] Li J-J, Zhang H-C. Stability and adaptive evolution of higher-order vector vortex solitons in thermally nonlinear media with tunable transverse size. Chaos Solitons Fractals 2023;177:114195.
[36] Liang G. Revolving and spinning of optical patterns by two coaxial spiraling elliptic beams in nonlocal nonlinear media. Opt Express 2019;27(10):14667–74.
[37] Zhang Z, Qiao X, Midya B, Liu K, Sun J, Wu T, Liu W, Agarwal R, Jornet JM, Longhi S, et al. Tunable topological charge vortex microlaser. Science 2020;368(6492):760–3.
[38] Molina-Terriza G, Torres JP, Torner L. Twisted photons. Nat Phys 2007;3(5):305–10.
[39] Kavokin A, Liew TC, Schneider C, Lagoudakis PG, Klembt S, Hoefling S. Polariton condensates for classical and quantum computing. Nat Rev Phys 2022;4(7):435–51.
[40] Abo-Shaeer JR, Raman C, Vogels JM, Ketterle W. Observation of vortex lattices in Bose–Einstein condensates. Science 2001;292(5516):476–9.
[41] Donadello S, Serafini S, Tylutki M, Pitaevskii LP, Dalfovo F, Lamporesi G, Ferrari G. Observation of solitonic vortices in Bose–Einstein condensates. Phys Rev Lett 2014;113(6):065302.
[42] Mihalache D. Localized structures in optical and matter-wave media: a selection of recent studies. Rom Rep Phys 2021;73(2):403.
[43] Wang P, Fu Q, Konotop VV, Kartashov YV, Ye F. Observation of localization of light in linear photonic quasicrystals with diverse rotational symmetries. Nat Photonics 2024;18(3):224–9.
[44] Shi A, Peng Y, Jiang J, Peng Y, Peng P, Chen J, Chen H, Wen S, Lin X, Gao F, et al. Observation of topological corner state arrays in photonic quasicrystals. Laser Photonics Rev 2024;18(7):2300956.
[45] Shi A, Peng Y, Peng P, Chen J, Liu J. Delocalization of higher-order topological states in higher-dimensional non-Hermitian quasicrystals. Phys Rev B 2024;110(1):014106.
[46] Yang K, Fu Q, Prates HC, Wang P, Kartashov YV, Konotop VV, Ye F. Observation of thouless pumping of light in quasiperiodic photonic crystals. Proc Natl Acad Sci 2024;121(47):e2411793121.
[47] Liu E, Liu J. Quasiperiodic photonic crystal fiber. Chin Opt Lett 2023;21(6):060603.
[48] Huo Z, Liu E, Liu J. Hollow-core photonic quasicrystal fiber with high birefringence and ultra-low nonlinearity. Chin Opt Lett 2020;18(3):030603.
[49] Ivanov S, Zhuravitskii S, Kostyuchenko N, Skryabin N, Dyakonov I, Kalinkin A, Kulik S, Kompanets V, Chekalin S, Alyatkin S, et al. Observation of light localization at the edges of quasicrystal waveguide arrays. Phys Rev Lett 2025;134(11):113803.
[50] Lahini Y, Pugatch R, Pozzi F, Sorel M, Morandotti R, Davidson N, Silberberg Y. Observation of a localization transition in quasiperiodic photonic lattices. Phys Rev Lett 2009;103(1):013901.
[51] Xie P, Zhang Z-Q, Zhang X. Gap solitons and soliton trains in finite-sized two-dimensional periodic and quasiperiodic photonic crystals. Phys Rev E 2003;67(2):026607.
[52] Ivanov SK, Konotop VV, Kartashov YV, Torner L. Vortex solitons in Moiré optical lattices. Opt Lett 2023;48(14):3797–800.
[53] Fu Q, Wang P, Huang C, Kartashov YV, Torner L, Konotop VV, Ye F. Optical soliton formation controlled by angle twisting in photonic Moiré lattices. Nat Photonics 2020;14(11):663–8.
[54] Wang L, Yan Z, Zhu Y, Zeng J. Dissipative gap solitons and vortices in Moiré optical lattices. Natl Sci Open 2024;3(6):20240011.
[55] Arkhipova A, Kartashov YV, Ivanov SK, Zhuravitskii S, Skryabin N, Dyakonov I, Kalinkin A, Kulik S, Kompanets VO, Chekalin S, et al. Observation of linear and nonlinear light localization at the edges of Moiré arrays. Phys Rev Lett 2023;130(8):083801.
[56] Zeng L, Malomed BA, Mihalache D, Li J, Zhu X. Solitons in composite linear–nonlinear Moiré lattices. Opt Lett 2024;49(24):6944–7.
[57] Kartashov YV, Ye F, Konotop VV, Torner L. Multifrequency solitons in commensurate-incommensurate photonic Moiré lattices. Phys Rev Lett 2021;127(16):163902.
[58] Wang P, Zheng Y, Chen X, Huang C, Kartashov YV, Torner L, Konotop VV, Ye F. Localization and delocalization of light in photonic Moiré lattices. Nature 2020;577(7788):42–6.
[59] Huang C, Shang C, Kartashov YV, Ye F. Vortex solitons in topological disclination lattices. Nanophotonics 2024;13(18):3495–502.
[60] Ablowitz MJ, Ilan B, Schonbrun E, Piestun R. Solitons in two-dimensional lattices possessing defects, dislocations, and quasicrystal structures. Phys Rev E—Stat Nonlinear Soft Matter Phys 2006;74(3):035601.
[61] Desyatnikov AS, Kivshar YS, Torner L. Chapter 5 - optical vortices and vortex solitons. In: Progress in optics, vol. 47, Elsevier; 2005, p. 291–391.
[62] Longhi S. Quantum-optical analogies using photonic structures. Laser Photon Rev 2009;3(3):243–61.
[63] Szameit A, Nolte S. Discrete optics in femtosecond-laser-written photonic structures. J Phys B 2010;43(16):163001.
[64] Kartashov YV, Malomed BA, Torner L. Solitons in nonlinear lattices. Rev Modern Phys 2011;83:247–305.
[65] Kartashov YV, Arkhipova A, Zhuravitskii S, Skryabin N, Dyakonov I, Kalinkin A, Kulik S, Kompanets VO, Chekalin S, Torner L, et al. Observation of edge solitons in topological trimer arrays. Phys Rev Lett 2022;128(9):093901.
[66] Ren B, Arkhipova AA, Zhang Y, Kartashov YV, Wang H, Zhuravitskii SA, Skryabin NN, Dyakonov IV, Kalinkin AA, Kulik SP, et al. Observation of nonlinear disclination states. Light: Sci Appl 2023;12(1):194.
[67] Zhong H, Kompanets VO, Zhang Y, Kartashov YV, Cao M, Li Y, Zhuravitskii SA, Skryabin NN, Dyakonov IV, Kalinkin AA, et al. Observation of nonlinear fractal higher order topological insulator. Light: Sci Appl 2024;13(1):264.
[68] Kompanets VO, Feng S, Zhang Y, Kartashov YV, Li Y, Zhuravitskii SA, Skryabin NN, Kireev AV, Dyakonov IV, Kalinkin AA, et al. Observation of nonlinear topological corner states originating from different spectral charges. Adv Mater 2025;2500556.
[69] Zhang B, Yan W, Chen F. Recent advances in femtosecond laser direct writing of three-dimensional periodic photonic structures in transparent materials. Adv Photon 2025;7(11):034002.
[70] Hu Z, Bongiovanni D, Jukić D, Jajtić E, Xia S, Song D, Xu J, Morandotti R, Buljan H, Chen Z. Nonlinear control of photonic higher-order topological bound states in the continuum. Light: Sci Appl 2021;10(1):164.
[71] Zhong H, Xia S, Zhang Y, Li Y, Song D, Liu C, Chen Z. Nonlinear topological valley Hall edge states arising from type-II Dirac cones. Adv Photonics 2021;3(5). 056001–056001.
[72] Chen Z, Liu X, Zeng J. Electromagnetically induced Moiré, optical lattices in a coherent atomic gas. Front Phys 2022;17(4):42508.

[73] Zhang Z, Wang R, Zhang Y, Kartashov YV, Li F, Zhong H, Guan H, Gao K, Li F, Zhang Y, et al. Observation of edge solitons in photonic graphene. Nat Commun 2020;11(1):1902.
[74] Du H, Zhao H, Li Y, Wang Y, Li R, Wu J, Liu W, Zhang Y, Xiao L, Jia S, Ma J. Observation of nonlinear edge states in an interacting atomic trimer array. Light: Sci Appl 2025;14(1):296.
[75] Rajan MM, Veni SS. Impact of external potential and non-isospectral functions on optical solitons and modulation instability in a cubic quintic nonlinear media. Chaos Solitons Fractals 2022;159:112186.
[76] Saravana Veni S, Mani Rajan MS, Bertrand Tabi C, Crépin Kofané T. Numerical investigation on nonautonomous optical Rogue waves and modulation instability analysis for a nonautonomous system. Phys Scr 2024;99(2):025202.
[77] Rutckaia V, Schilling J. Ultrafast low-energy all-optical switching. Nat Photonics 2020;14(1):4–6.
[78] Yang M, Zhang H-Q, Liao Y-W, Liu Z-H, Zhou Z-W, Zhou X-X, Xu J-S, Han Y-J, Li C-F, Guo G-C. Topological band structure via twisted photons in a degenerate cavity. Nat Commun 2022;13(1):2040.
[79] Zhang Y, Bongiovanni D, Wang Z, Wang X, Xia S, Hu Z, Song D, Jukić D, Xu J, Morandotti R, Buljan H, Chen Z. Realization of photonic *p*-orbital higher-order topological insulators. ELight 2023;3(1):5.
[80] He C, Zhao L, Zhang S, Zhou L, Ma S. Intrinsic topological hinge states induced by boundary gauge fields in photonic metamaterials. ELight 2025;5(1):19.
[81] Peng R, Yang K, Fu Q, Chen Y, Wang P, Kartashov YV, Konotop VV, Ye F. Topological pumping of light governed by Fibonacci numbers. ELight 2025;5(1):16.